Lifetime Spectroscopy Investigation of Light-Induced Degradation in *p*-type Multicrystalline Silicon PERC

Ashley E. Morishige, Mallory A. Jensen, David Berney Needleman, Kenta Nakayashiki, Jasmin Hofstetter, Tsu-Tsung Andrew Li, and Tonio Buonassisi, *Member, IEEE*

***Abstract*—When untreated, light-induced degradation (LID) of *p*-type multicrystalline silicon (mc-Si)-based passivated emitter and rear cell (PERC) modules can reduce power output by up to 10% relative during sun-soaking under open-circuit conditions. Identifying the root cause of this form of LID has been the subject of several recent investigations. Lifetime spectroscopy analysis, including both injection and temperature dependencies (IDLS and TIDLS), may offer insight into the root-cause defect(s). In this paper, to illustrate the root-case defect identification method, we apply room-temperature IDLS to intentionally Cr-contaminated mc-Si. Then, we apply this technique to the *p*-type mc-Si that exhibits LID in PERC devices, and we provide further insights by analyzing qualitatively the injection-dependent lifetime as a function of temperature. We quantify the sensitivity of the capture cross-section ratio to variations in the measured lifetime curve and in the surface recombination. We find that the responsible defect most likely has an energy level between 0.3 and 0.7 eV above the valence band and a capture cross-section ratio between 26 and 36. Additionally, we calculate the concentrations of several candidate impurities that may cause the degradation.**

***Index Terms*—Bulk lifetime, lifetime spectroscopy, light-induced degradation (LID), LeTID, multicrystalline silicon (mc-Si), passivated emitter and rear cell (PERC), temperature- and injection-dependent lifetime spectroscopy (TIDLS).**

I. Introduction

PASSIVATED emitter and rear cells (PERC) offer theoretical cost advantages relative to the current industry standard aluminum back-surface field (Al-BSF) devices [1]. However, PERC devices incorporating certain types of *p*-type multicrystalline silicon (mc-Si) wafers exhibit light-induced degradation (LID), in severe cases reducing power output at the maximum power point by more than 10% relative [2]–[9]. Developing engineering solutions and identifying the root cause(s) for this LID may accelerate industrial adoption of PERC, with projected manufacturing cost savings ($/W).

Several engineering solutions for *p*-type mc-Si PERC LID have been devised, including modifying the mc-Si wafer type, modifying the metallization firing time–temperature profile, and accelerated degradation and regeneration [7]–[9]. Evidence exists for the root-cause defect having a strong bulk component, being spread throughout the wafer, and being reversible [7]. Possible root-cause candidates include a deep-level donor point defect, a charged nanoprecipitate, a charged structural defect, or hydrogen associating and dissociating with impurity point defects [7]. However, a clear consensus has yet to emerge regarding the cause of the observed *p*-type mc-Si PERC LID.

Previous work has described the theory of lifetime spectroscopy [10], [11] and demonstrated it using intentionally contaminated samples [11]–[26]. Many of the reported studies utilize both the temperature- and injection-dependence of minority carrier lifetime or a known metastability to pinpoint the nature of the defects in their intentionally contaminated materials. However, a single injection-dependent lifetime curve can be used to gain insight into the possible defect parameters [10], [11], [25]. Furthermore, Murphy *et al.* proposed a linear parameterization of the Shockley–Read–Hall (SRH) equations which simplifies the interpretation and fitting of measured data [17]. These lifetime spectroscopy techniques, while robust, have not yet been universally adopted for the identification of defects in industrial (not intentionally contaminated) materials.

In this paper, we combine defect-targeted and injection-dependent lifetime spectroscopy (IDLS) with the simplified linear parameterization to perform root-cause analysis of *p*-type mc-Si PERC LID. To explain our approach, which combines several tools reported in the literature, we first apply room-temperature IDLS to an example of intentionally chromium-contaminated *p*-type mc-Si. We then apply IDLS to an industrial sample set for which there are many unknowns. We analyze degraded and undegraded *p*-type mc-Si PERC semifabricates. We report the concentrations of candidate root-cause impurities, and we quantify the error in the analysis, bounding the parameter space of the possible root cause(s) of *p*-type mc-Si PERC LID. We further extend our analysis by considering qualitatively the injection-dependent lifetime of degraded semifabricates as a function of temperature (TIDLS).

Manuscript received June 21, 2016; revised August 12, 2016; accepted August 18, 2016. This work was supported by the National Science Foundation (NSF) and the Department of Energy under NSF CA No. EEC-1041895 and the National Research Foundation Singapore through the Singapore Massachusetts Institute of Technology (MIT) Alliance for Research and Technology's "low energy electronic systems IRG" research. This work made use of the Center for Nanoscale Systems, Harvard University, supported by NSF Award ECS-0335765. The work of D. Berney Needleman was supported by the U.S. Department of Defense NDSEG Graduate Research Fellowship. The work of M. A. Jensen was supported by the NSF Graduate Research Fellowship under Grant 1122374. A. E. Morishige and M. A. Jensen contributed equally to this work.

A. E. Morishige, M. A. Jensen, D. Berney Needleman, J. Hofstetter, and T. Buonassisi are with the Massachusetts Institute of Technology, Cambridge, MA 02139 USA (e-mail: aemorish@alum.mit.edu; jensenma@mit.edu; davidbn@alum.mit.edu; jasmin.hofstetter@gmx.de; buonassisi@mit.edu).

K. Nakayashiki is with the Renewable Energy Corporation Solar Pte. Ltd., Singapore 637312 (e-mail: kenta.nakayshiki@recgroup.com).

T. A. Li is with Gyana Limited, London SE1 9SG, U.K. (e-mail: andrew.li@gyana.space).

Color versions of one or more of the figures in this paper are available online at http://ieeexplore.ieee.org.

Digital Object Identifier 10.1109/JPHOTOV.2016.2606699

II. Methods: Injection-Dependent Lifetime Spectroscopy

IDLS analysis can most effectively enable root-cause defect identification when the following conditions are met.

1) The material can be reasonably assumed to be dominated by one or two defects.
2) The defect(s) are uniformly distributed or injection-dependent lifetime can be measured at the same spatial resolution as changes in the defect distribution [16].
3) Other recombination mechanisms are small or well known in comparison in the measured injection range.
4) Recombination at the defect can be modeled as SRH recombination [27], [28], and the underlying defect has been well characterized in the literature in terms of its SRH parameters.

Herein, we apply IDLS according to the following steps.

1) Measure spatially-averaged injection-dependent lifetime.
2) Calculate the intrinsic lifetime, including the Auger and radiative components [29].
3) Assess the surface-related lifetime.
4) Extract the SRH-related lifetime from the measured lifetime by harmonically subtracting the intrinsic and surface lifetime components.
5) Plot the SRH lifetime as a function of a linearized carrier concentration (the ratio of electron to hole concentrations, denoted by the variable *X*) [17].
6) Fit the lifetime versus *X* curve on linear axes with one or more lines, according to the expected number of defects, which combine in a harmonic sum to minimize the mean squared error.
7) From the slope and *y*-intercept of the fitted lines, calculate the ratio of electron to hole capture cross-sections as a function of the energy level, *k* versus $E_{t,}$ to identify root-cause defect candidates [10], [11], [26], [30].
8) In addition, from the fitted line parameters, calculate the electron capture cross-section as a function of the defect energy level to quantify the concentration of candidate defects with known capture cross-sections [10], [17].

The equations for steps (5), (7), and (8) for *p*-type Si adapted from [17] are shown in (1)–(3). *k* is the ratio of electron to hole capture cross-sections. σ_e is the electron capture cross section. *Q* is a parameter defined in (3) and also reported in [16], [17]. v_{th} is the thermal velocity of carriers in Si. *N* is the concentration of the defect. τ is the minority carrier lifetime. *X* is the ratio of electron to hole concentrations. p_0 is the equilibrium hole concentration, determined from the measured resistivity. n_1 and p_1 are the SRH carrier concentrations, which are a function of the energy level, E_t, and the density of states in the conduction and valence bands. The defect is assumed to lie within the bandgap, with known possible E_t from 0 to 1.124 eV above the valence band.

$$k = \frac{v_{\mathrm{th,holes}}}{v_{\mathrm{th,electrons}}} Q \tag{1}$$

$$\sigma_e N_t \; v_{\mathrm{th,electrons}} = \frac{1}{\tau_{n\,X\to 0}} \left(1 + \frac{1}{p_0}\big(Q\; n_1 + p_1\big)\right) \tag{2}$$

$$Q = \frac{\frac{d\tau_n}{dX}/\tau_{n\,X\to 1} + \frac{p_1}{p_0}}{1 - \frac{n_1}{p_0} - \frac{d\tau_n}{dX}/\tau_{n\,X\to 1}}. \tag{3}$$

We choose quasi-steady-state photoconductance (QSSPC) [31] using the Sinton Instruments WCT-120 for the lifetime measurements because it is the most established way to measure the injection dependence of minority carrier lifetime, and it is also the lifetime measurement method used by Murphy *et al.* [17] for the lifetime spectroscopy and subsequent linearization and fitting procedure.

The lifetime measurements are performed on mc-Si, which is known to be spatially inhomogeneous in lifetime (e.g., structural defects, precipitated metals). The effect of lifetime inhomogeneity on quantitative defect concentration measurements by QSSPC has been reported by Geerligs *et al.* [32]. They studied a model defect sample: a single-crystalline silicon wafer that was implanted with iron and annealed, then half coated with an optimized passivation layer and half unpassivated (i.e., long and short effective lifetimes, respectively). Using the crossover method for Fe-B pair quantification, they found a maximum of two times relative difference in Fe concentration by measuring the "half-and-half sample" in different locations. However, the slopes of the QSSPC curves measured (see [32, Fig. 4]) were similar to within 5% (for Fe-B) and 20% (for $\mathrm{Fe_i}$), measured between 1×10^{14} and 1×10^{15} $\mathrm{cm^{-3}}$ injection levels. The E_t versus *k* curves are determined by the shape (slope) of the injection-dependent lifetime curve. Therefore, we conclude that the defect identification in the mc-Si samples studied herein is relatively insensitive to the lifetime heterogeneity introduced by structural defects.

III. Case Study: Intentionally Contaminated Multicrystalline Silicon

To illustrate the root-cause IDLS analysis approach described in the previous section, we analyze an intentionally Cr-contaminated *p*-type mc-Si wafer with a known total Cr concentration of 9.9×10^{13} $\mathrm{cm^{-3}}$ and an interstitial Cr (Cr_i) concentration of 4.5×10^{13} $\mathrm{cm^{-3}}$ measured by $\mathrm{Cr}_i - \mathrm{B}_s$ pair dissociation. See Jensen *et al.* [33] for further sample and experimental details.

For this low-lifetime sample passivated with AlO_x, the measured lifetime is strongly dominated by SRH recombination. Thus, the injection-dependent SRH lifetime is taken to be the measured lifetime with the intrinsic lifetime component removed. The linearized SRH curve is shown in Fig. 1. From the linearized curve, two distinct slopes, one at low injection ($X < 0.01$) and one at higher injection ($X > 0.01$) are visible. Thus, two lines are fit. The dominant defect over the majority of the injection range (dashed line) has a slope of 0.412 μs and a *y*-intercept of 0.147 μs while the secondary defect (dotted line) has a slope of 40.2 μs and a *y*-intercept of 1.63×10^{-4} μs.

For the dominant defect (shallower dashed line in Fig. 1), (1) and (3) are applied to determine possible *k* values as a function of the energy level, E_t. The k–E_t curve for this defect is shown in Fig. 2 with some known literature values of impurities in silicon for comparison [23], [24], [34]–[37]. Consistent with

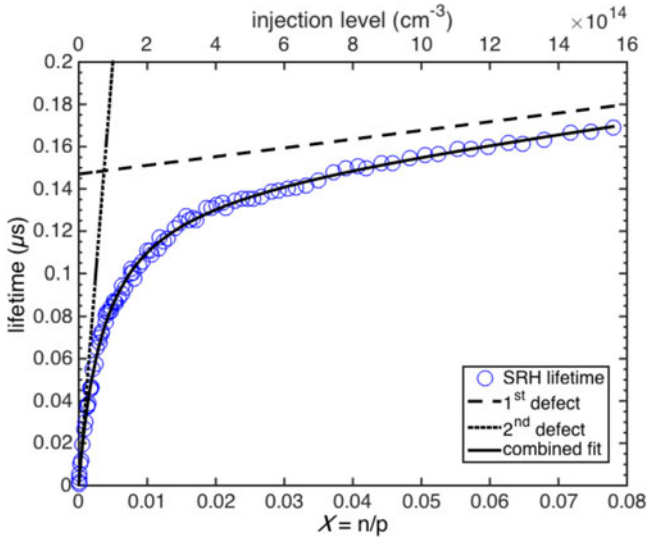

Fig. 1. Injection-dependent minority carrier lifetime for an intentionally Cr-contaminated *p*-type mc-Si wafer. The SRH lifetime curve is shown in open blue circles. Two linear fits to the linearized SRH curve (dotted line and dashed line) and their combination (solid line) are also shown.

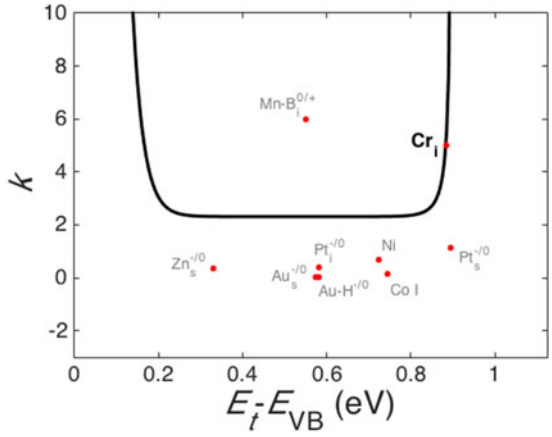

Fig. 2. Capture cross-section ratio *k* as a function of energy level E_t above the valence band for the dominant defect in the Cr-contaminated sample. Defects with parameters from literature are plotted with red dots and labeled in gray or black [23], [24], [34]–[37]. The $k - E_t$ curve directly intersects the literature value for Cr_i.

the intentional introduction of Cr in the melt during growth of this wafer, the extracted curve intersects the literature value for interstitial chromium Cr_i, with $k = 5$ and $E_t = 0.88$ eV [24].

From the dominant defect curve, we also plot the electron capture cross-section as a function of the energy level (see Fig. 3, *x*-axis) and impurity concentration (see Fig. 3, colored curves) as described by (2) and (3). Identified as a possible lifetime-limiting defect in Fig. 2, Cr_i is plotted. Given that the electron capture cross-section for Cr_i is 2×10^{-14} cm^2 [24], the calculated concentration of Cr_i is 2.78×10^{13} cm^{-3}, which is within 40% of the value measured by $\mathrm{Cr}_i - \mathrm{B}_s$ dissociation in [33]. For this sample, we know that Cr was introduced during growth and that Cr is present in a high enough concentration to form precipitates at grain boundaries [33]. If there were multiple candidates

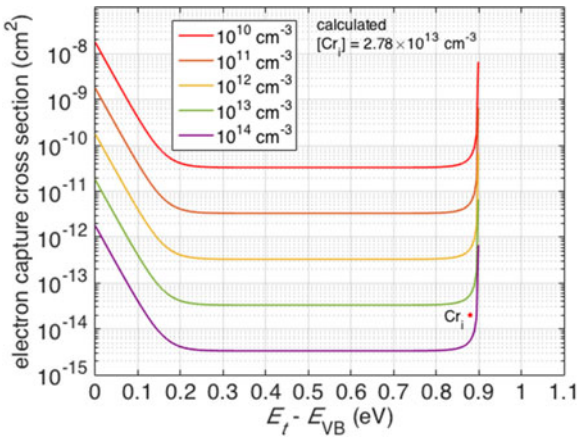

Fig. 3. Electron capture cross-section as a function of energy level E_t above the valence band for the dominant defect in the Cr-contaminated sample. Cr_i with parameters from literature is plotted [24]. The calculated $[\mathrm{Cr}_i]$ is 2.78×10^{13} cm^{-3}.

determined from the $k - E_t$ relationship, we could combine the results of Fig. 3 with total impurity concentration measurements (e.g., inductively coupled plasma mass spectrometry) to rule out certain candidates.

Similar to previously reported studies, this case study of an intentionally introduced, known defect with independent measurements of the defect concentration and SRH parameters in the literature demonstrates the robustness of this technique for a *p*-type mc-Si wafer that meets the requirements outlined in Section II. We now apply this same method to an industrially important case with many more unknowns: *p*-type mc-Si PERC LID.

IV. Injection-Dependent Lifetime Spectroscopy Analysis of *p*-type Multicrystalline Silicon Passivated Emitter and Rear Cell Light-Induced Degradation

The samples analyzed in this section are *p*-type mc-Si PERC semifabricates fired at 950 °C peak temperature without the contact metal present. From top to bottom, the semifabricates are comprised of an SiN_x layer, phosphorus-diffused emitter, *p*-type mc-Si wafer, a passivation layer, and a capping layer. One wafer was fired and then stored in the dark (undegraded) while the other was fired and then light soaked at a temperature of 65–75 °C with an illumination of 0.9–1.1 suns for one week (degraded). See Nakayashiki *et al.* [7] for further details about the module-level degradation and experimental details for these specific wafers. IDLS is a promising root-cause defect analysis tool for PERC LID because a clear injection-dependent lifetime signature can be observed for a degraded sample [6]–[8]. Furthermore, the degradation has been shown to be repeatable, somewhat predictable (even though the exact cause is currently unknown to the community), and is ubiquitous across the wafer (see μ-PCD maps in [7, Fig. 8]). Accordingly, injection-dependent lifetimes measured at several different locations within the degraded wafer were found to be nearly identical. For these reasons, we hypothesize that the degraded lifetime should be due to at most two or three dominant defects.

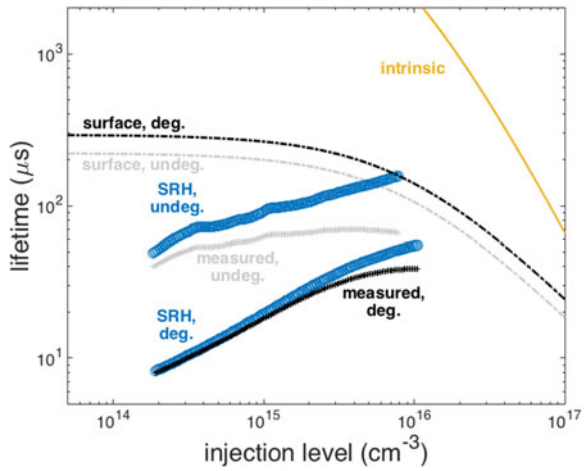

Fig. 4. Lifetime components for p-type mc-Si PERC LID wafers fired at 950 °C before (gray) and after (black) degradation. The intrinsic lifetime (yellow) is the same for both samples. The surface lifetime is denoted by the dash-dotted lines. The extracted SRH lifetime is denoted in the blue open circles. The measured lifetime is denoted by the lines of $+$'s below the SRH lifetime curves.

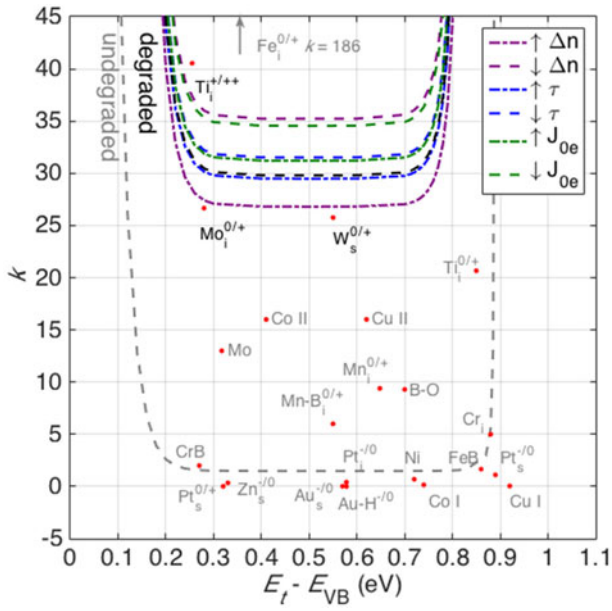

Fig. 5. Capture cross-section ratio k as a function of energy level E_t above the valence band for the dominant defects in the 950 °C peak firing condition in the undegraded (gray curve) and degraded (black curve) states. Defects with parameters from literature [20], [23], [24], [34]–[37], [40], [41] are plotted with red dots and labeled in either gray or black. Black labeled defects are possible candidates for the root cause of the PERC LID observed in this study. The measured injection level (purple) and measured lifetime (blue) were increased or decreased by 10%, and J_{0e} (green) was increased or decreased by 30% relative to the base values.

The room-temperature injection-dependent SRH lifetime curves (blue open circles) are extracted from the measured lifetime curves (plus signs) by removing the intrinsic (yellow) and surface (dash-dotted line) lifetime components for the undegraded and the degraded samples (see Fig. 4). From a fit to the measured injection-dependent lifetime curves in a high injection as described in [38], the undegraded wafer has an emitter recombination current $J_{0e} = 6.47 \times 10^{-14}$ A/cm^2 at an injection level of 2.5×10^{16} cm^{-3} and the degraded wafer has $J_{0e} = 4.9 \times 10^{-14}$ A/m^2 at an injection level of 1.9×10^{16} cm^{-3}. We note uncertainty for the J_{0e} estimations due to the asymmetric structure of the semifabricates and a maximum measured injection level that is close to the sample doping level. The impact of this uncertainty will be addressed in the following paragraphs. The degraded curve is dominated by the SRH lifetime throughout much of the measured injection range, but the undegraded curve is influenced by both surface and SRH lifetime and, therefore, characterization of the surface component is important.

From the linearized SRH curves, more than one slope is visible. Thus, two lines are fit, and their combination matches the measured curve well [7]. For both the undegraded and degraded samples, there is one defect that dominates throughout the entire injection level range. For the undegraded sample, the dominant defect has a slope of 162 μs and a y-intercept of 90 μs while the secondary defect has a slope of 6086 μs and a y-intercept close to 0 μs. For the degraded sample, the secondary defect has a slope close to 0 μs and a y-intercept of 117 μs while the dominant defect has a slope of 186 μs and a y-intercept of 5.1 μs.

For the dominant defect curve in each state, we calculate k as a function of E_t as in (1) and (3). The resulting curves are shown in Fig. 5. It is clear that the lifetime-limiting defects in the undegraded and the degraded states are distinct. Therefore, we focus on analysis of the degraded curve to gain insight into the cause of PERC LID.

To quantify the robustness of the k–E_t curve in the degraded state to experimental uncertainty, we performed a sensitivity analysis. To quantify the sensitivity to the surface lifetime calculation, the J_{0e} was increased and decreased by 30%, one standard deviation from the mean of the J_{0e} measured on five similar samples. To quantify the sensitivity to inaccuracies in the measured injection-dependent lifetime curve, the measured injection level was increased and decreased by 10%, and the measured lifetime was increased and decreased by 10%. These variations account for uncertainties in thickness, resistivity, and optical properties, and are approximately the same as the reported laboratory-to-laboratory reproducibility for QSSPC measurements [39]. For each perturbation, the linearized SRH lifetime and the $k - E_t$ curves were recalculated (see Fig. 5).

For the degraded wafer, the perturbations result in a range of k values between 26 and 36 in the middle flat portion of the $k - E_t$ curve. The $k - E_t$ curve is most sensitive to the changes in injection level (purple curves, $k = 26.8$ and 35.2 at midgap) and J_{0e} (green curves, $k = 31.2$ and 34.6 at midgap). On the other hand, the $k - E_t$ curve is much less sensitive to changes in the absolute value of the lifetime (blue curves, $k = 29.5$ and 31.5 at midgap) due to the fact that SRH recombination dominates the measured lifetime compared to both surface and intrinsic contributions. This sensitivity analysis demonstrates that the defect identification by IDLS analysis is quite robust. The same analysis applied to the undegraded wafer also showed that the uncertainty does not affect the conclusion that the lifetime-limiting defects are distinctly different between the two states. Based

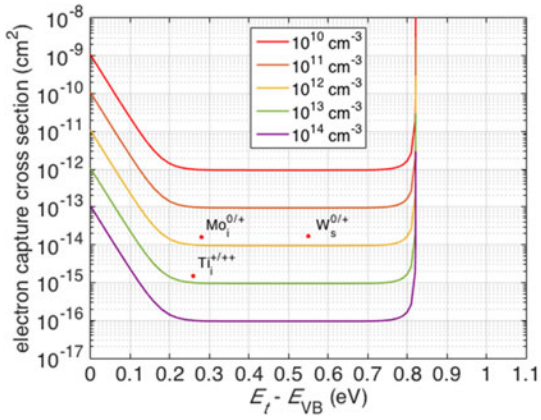

Fig. 6. Electron capture cross-section as a function of energy level above the valence band for several concentrations of the dominant defect in the 950 °C firing condition in the degraded state. Candidate defects are identified by the $k - E_t$ curves in Fig. 5. The calculated candidate concentrations are $[\mathrm{Ti}_i^{+/++}] = 6.6 \times 10^{12}\ \mathrm{cm}^{-3}$, $[\mathrm{Mo}_i^{0/+}] = 6.1 \times 10^{11}\ \mathrm{cm}^{-3}$, and $[\mathrm{W}_{s\,0/+}] = 5.6 \times 10^{11}\ \mathrm{cm}^{-3}$.

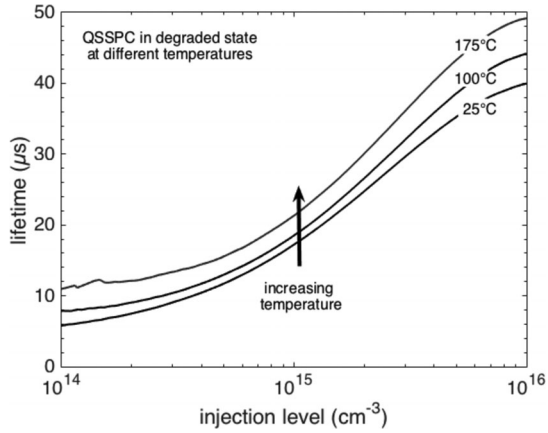

Fig. 7. Injection-dependent lifetime curves for the degraded state measured at 25, 100, and 175 °C. The shapes of the curves are fairly similar with lifetime increasing as injection level increases. The trends in calculated SRH lifetime shape match the measured temperature-dependent curves well for $E_t = 0.3$ to 0.7 eV above the valence band. We cannot rule out defects with $E_t =$ 0.0–0.1, 0.22 – 0.3, and 0.7 – 0.75 eV above the valence band.

on these results, we therefore add to our previous conclusion, in which we gave a single k value [7], to state that, if the LID defect level is near the middle of the bandgap, the k value lies between 26 and 36.

For comparison, defects with values of k and E_t available in the literature are plotted with the curves in Fig. 5 [20], [23], [24], [33]–[37], [40], [41]. Other defects with parameters available in the literature that lie outside the bounds of the axes in Fig. 5 do not lie near the calculated curves and are thus excluded. It should be noted that the defect parameters vary widely in the literature for some defects, and not all the parameters are known for some defects, thus increasing uncertainty in the defect identification via IDLS. Using the literature values cited herein, some candidates for lifetime-limiting impurities in the degraded state are the Ti interstitial double donor [20], [41], the Mo interstitial donor [37], and the W substitutional donor [40].

The electron capture cross section as a function of the energy level was also calculated for a wide range of defect concentrations (see Fig. 6) according to (2), and the top three candidates from Fig. 5 were plotted with the curves. We note that the injection-dependent lifetime curves may be affected by the presence of structural defects, introducing some error into the calculation of the concentrations of possible candidate impurities; nonetheless, we are confident that the lifetime is primarily limited by the degradation-related defect, so we directly analyze the SRH lifetime data shown in Fig. 4. The calculated point defect concentrations are $[\mathrm{Ti}_i^{+/++}] = 6.6 \times 10^{12}\ \mathrm{cm}^{-3}$, $[\mathrm{Mo}_i^{0/+}] = 6.1 \times 10^{11}\ \mathrm{cm}^{-3}$, and $[\mathrm{W}_s^{0/+}] = 5.6 \times 10^{11}\ \mathrm{cm}^{-3}$. ICP-MS data are not available for these specific samples, but for comparison, we consult the ICP-MS measurements of total element concentrations provided in [8] and in the supplementary information of [42]. In [8], $[\mathrm{Ti}] = 3.26 \times 10^{14}\ \mathrm{cm}^{-3}$, $[\mathrm{Mo}] = 6.45 \times 10^{12}\ \mathrm{cm}^{-3}$, and $[\mathrm{W}] = 1.58 \times 10^{14}\ \mathrm{cm}^{-3}$. In [42], in the bulk of 6N's upgraded metallurgical grade mc-Si wafers, $[\mathrm{Mo}] = 10^{12}\ \mathrm{cm}^{-3}$ and $[\mathrm{W}] = 10^{13}\ \mathrm{cm}^{3}$. The concentrations of metal impurities can vary up to two orders of magnitude for different types of mc-Si for photovoltaics. Thus, the impurity concentrations calculated from the IDLS analysis are reasonable.

This room-temperature IDLS analysis significantly narrows the possible candidates for the root-cause defect of *p*-type mc-Si PERC LID. In addition to confirming the highly asymmetric nature of carrier capture for the PERC LID defect, we note from Fig. 6, for example, that $10^{-15}\ \mathrm{cm}^2$ is a reasonable lower bound on the electron capture cross section for the dominant defect. For defects with E_t between 0.25 and 0.75 eV, this lower bound corresponds to a point defect concentration of $10^{13}\ \mathrm{cm}^{-3}$, which is a reasonable upper bound on the point defect impurity concentration given the total impurity concentrations measured by ICP-MS.

Temperature-dependent QSSPC measurements [22] and analysis can further narrow the range of candidates to a specific $k - E_t$ pair. In general, the injection-dependent SRH lifetime can increase, decrease, or remain unchanged as the injection level increases [11]. The E_t, k, and temperature, among other factors, affect the shape of the curve. For example, as the temperature increases, the lifetime curves can increase in magnitude and, then, maintain their shape or flatten and become inverted. In Fig. 7, we show QSSPC measurements of the injection-dependent lifetime in the degraded state measured at three different set point temperatures: 25, 100, and 175 °C. We observe that all three curves have similar shape. As the temperature increases, the lifetime increases, and as the injection level increases, the lifetime increases.

We calculated the expected shapes of the injection-dependent SRH lifetime curves as a function of temperature according to the models described in [10], assuming a single defect for each of the $k - E_t$ pairs along the $k - E_t$ curve calculated for the degraded state (see Fig. 5, black dashed line). We found that the trends in calculated SRH lifetime shape match the measured curves well for $E_t = 0.3$–0.7 eV above the valence band. We cannot rule out defects with $E_t =$ 0.0–0.1, 0.22–0.3, and 0.7–0.75 eV above the valence band. The possible capture cross-section ratios are paired with the possible energy levels

via the $k - E_{\mathrm{t}}$ curve. This analysis indicates that it is less likely that either Ti interstitial double donor or Mo interstitial donor is the responsible defect compared to W substitutional donor, according to the $k - E_t$ values reported in Fig. 5.

Finally, we also observe that after the temperature-dependent measurements up to 200 °C, the lifetime remeasured at 25 °C is higher than its original value. This temperature-dependent behavior is consistent with previous observations that the lifetime degradation can be reversed by a short anneal [7]. The instability of the lifetime can provide further insight into the nature of the defect.

This preliminary temperature analysis assumes that k is constant with temperature, which is not always the case [18], [20], [21], and it also assumes that the defect that is dominant at room temperature remains dominant at 100 and 175 °C. Additionally, we acknowledge that the surface recombination changes with temperature, but we see from Fig. 4 that the lifetime is dominated by SRH in low and medium injection. We assume that this condition holds as temperature increases and interpret the shape of the measured curve.

Measurement of injection-dependent SRH lifetime curves in a wider temperature range combined with detailed TIDLS analysis may further constrain the parameter space. Once the $k - E_t$ curve is further constrained, a root-cause defect that is consistent with the identified defect parameters and the module- and cell-level and other time- and temperature-dependent behavior (e.g., regeneration [6]) must still be described. Injection-dependent lifetime measurements taken as the degradation progresses may also provide insight into these behaviors.

V. Conclusions

We apply both IDLS and TIDLS to identify and quantify the concentration of impurities in 1) intentionally Cr-contaminated *p*-type mc-Si model samples and 2) *p*-type mc-Si that exhibited PERC LID. Through the analysis of the model samples, we illustrate our use of room-temperature IDLS in a root-cause analysis. We further investigate the nature of the defect by analyzing the injection-dependent lifetime of degraded samples as a function of temperature. The lifetime analysis of the *p*-type mc-Si PERC LID wafers shows that in the degraded state the responsible defect most likely has an energy level between 0.3 and 0.7 eV above the valence band and a capture cross-section ratio between 26 and 36. These data are consistent with a deep-level donor point defect, a charged nanoprecipitate, a charged structural defect, or hydrogen associating and dissociating with an impurity point defect (possibly substitutional W at a concentration of $\sim 5.6 \times 10^{11}\,\mathrm{cm}^{-3}$). We demonstrate that this analysis is robust to perturbations in the measured injection-dependent lifetime curve and emitter recombination current estimates. Thus, IDLS is a rapid and powerful analysis method for identifying and quantifying lifetime-limiting defects in PV systems. We note that as device architectures that involve high-temperature processing steps improve and wafer thicknesses decrease, higher injection levels are expected, suggesting that a continuously improving LID mitigation strategy that directly targets the root-cause defect(s) is advised.

Acknowledgment

The authors would like to thank R. Sinton and A. Blum for assistance with the temperature-dependent lifetime measurements. They also thank G. Coletti for providing the intentionally Cr-contaminated mc-Si wafers.

References

[1] P. A. Basore, "Understanding manufacturing cost influence on future trends in silicon photovoltaics," *IEEE J. Photovolt.* vol. 4, no. 6, pp. 1477–1482, Nov. 2014.

[2] K. Ramspeck *et al.*, "Light induced degradation of rear passivated mc-Si solar cells," in *Proc. 27th Eur. Photovolt. Solar Energy Conf. Exhib.*, Sept. 24–28, 2012, pp. 861–865.

[3] F. Fertig, K. Krauß, and S. Rein, "Light-induced degradation of PECVD aluminium oxide passivated silicon solar cells," *Phys. Status Solidi RRL – Rapid Res. Lett.*, vol. 9, no. 1, pp. 41–46, Jan. 2015.

[4] K. Krauß, F. Fertig, D. Menzel, and S. Rein, "Light-induced degradation of silicon solar cells with aluminium oxide passivated rear side," *Energy Procedia*, vol. 77, pp. 599–606, Aug. 2015.

[5] F. Fertig *et al.*, "The BOSCO solar cell: Simulation and experiment," *IEEE J. Photovolt.*, vol. 4, no. 5, pp. 1243–1251, Sep. 2014.

[6] F. Kersten *et al.*, "Degradation of multicrystalline silicon solar cells and modules after illumination at elevated temperature," *Sol. Energy Mater. Sol. Cells*, vol. 142, pp. 83–86, 2015.

[7] K. Nakayashiki *et al.*, "Engineering solutions and root-cause analysis for light-induced degradation in p-type multicrystalline silicon PERC modules," *IEEE J. Photovolt.*, vol. 6, no. 4, pp. 860–868, Jul. 2016.

[8] D. Bredemeier, D. Walter, S. Herlufsen, and J. Schmidt, "Lifetime degradation and regeneration in multicrystalline silicon under illumination at elevated temperature," *AIP Adv.*, vol. 6, 2016, Art. no. 035119.

[9] D. N. R. Payne *et al.*, "Acceleration and mitigation of carrier-induced degradation in p-type multi-crystalline silicon," *Phys. Status Solidi RRL*, vol. 10, no. 3, pp. 237–241, 2016.

[10] S. Rein, *Lifetime Spectroscopy: A Method of Defect Characterization in Silicon for Photovoltaic Applications.* New York, NY, USA: Springer, 2005.

[11] S. Rein, W. Warta, and S. W. Glunz, "Lifetime spectroscopy for defect characterization: Systematic analysis of the possibilities and restrictions," *J. Appl. Phys.*, vol. 91, 2002, Art. no. 2059.

[12] S. Rein and S. W. Glunz, "Electronic properties of the metastable defect in boron-doped Czochralski silicon: Unambiguous determination by advanced lifetime spectroscopy," *Appl. Phys. Lett.*, vol. 82, no. 7, pp. 1054–1056, 2003.

[13] D. Macdonald and L. J. Geerligs, "Recombination activity of interstitial iron and other transition metal point defects in p- and n-type crystalline silicon," *Appl. Phys. Lett.*, vol. 85, no. 18, pp. 4061–4063, 2004.

[14] D. Macdonald, A. Cuevas, and J. Wong-Leung, "Capture cross sections of the accepter level of iron-boron pairs in p-type silicon by injection-level dependent lifetime measurements," *J. Appl. Phys.*, vol. 89, 2001, Art. no. 7932.

[15] D. Macdonald, P. Rosenits, and P. N. K. Deenapanray, "Recombination activity of manganese in p- and n-type crystalline silicon," *Semicond. Sci. Technol.*, vol. 22, pp. 163–167, 2007.

[16] L. Mundt *et al.*, "Spatially resolved impurity identification via temperature- and injection-dependent photoluminescence imaging," *IEEE J. Photovolt.*, vol. 5, no. 5, pp. 1503–1509, Sep. 2015.

[17] J. D. Murphy, K. Bothe, R. Krain, V. V. Voronkov, and R. J. Falster, "Parameterization of injection-dependent lifetime measurements in semiconductors in terms of Shockley-Read-Hall statistics: An application to oxide precipitates in silicon," *J. Appl. Phys.*, vol. 111, 2012, Art. no. 113709.

[18] B. B. Paudyal, K. R. McIntosh, and D. Macdonald, "Temperature dependent electron and hole capture cross sections of iron-contaminated boron-doped silicon," in *Proc. 34th IEEE Photovolt. Spec. Conf.*, 2009, pp. 1588–1593.

[19] B. Paudyal, Y. H. Yoon, D. Cornwell, P. Shaw, and F. Machuca, "Identification of metal impurities in crystalline silicon wafers," in *Proc. IEEE Photovolt. Spec. Conf.*, 2011, pp. 437–441.

[20] B. B. Paudyal, K. R. McIntosh, and D. H. Macdonald, "Temperature dependent carrier lifetime studies on Ti-doped multicrystalline silicon," *J. Appl. Phys.*, vol. 105, 2009, Art. no. 124510.

[21] B. B. Paudyal, K. R. McIntosh, D. H. Macdonald, and G. Coletti, "Temperature dependent carrier lifetime studies of Mo in crystalline silicon," *J. Appl. Phys.*, vol. 107, 2010, Art. no. 054511.

[22] B. B. Paudyal, K. R. McIntosh, D. H. Macdonald, B. S. Richards, and R. A. Sinton, "The implementation of temperature control to an inductive-coil photoconductance instrument for the range of 0-230°C," *Prog. Photovolt.: Res. Appl.*, vol. 16, pp. 609–613, 2008.
[23] T. Roth *et al.*, "Electronic properties and dopant pairing behavior of manganese in boron-doped silicon," *J. Appl. Phys.*, vol. 102, 2007, Art. no. 103716.
[24] J. Schmidt, R. Krain, K. Bothe, G. Pensl, and S. Beljakowa, "Recombination activity of interstitial chromium and chromium-boron pairs in silicon," *J. Appl. Phys.*, vol. 102, 2007, Art. no. 123701.
[25] W. Warta, "Defect and impurity diagnostics and process monitoring," *Sol. Energy Mater. Sol. Cells*, vol. 72, pp. 389–401, 2002.
[26] C. Sun, F. E. Rougieux, and D. Macdonald, "Reassessment of the recombination parameters of chromium in n- and p-type crystalline silicon and chromium-boron pairs in p-type crystalline silicon," *J. Appl. Phys.*, vol. 115, 2014, Art. no. 214907.
[27] W. Shockley and W. T. Read Jr., "Statistics of the recombination of holes and electrons," *Phys. Rev.*, vol. 87, 1952, Art. no. 835.
[28] R. N. Hall, "Electron-hole recombination in germanium," *Phys. Rev.*, vol. 87, p. 387, 1952.
[29] A. Richter, F. Werner, A. Cuevas, J. Schmidt, and S. W. Glunz, "Improved parameterization of auger recombination in silicon," *Energy Procedia*, vol. 27, pp. 88–94, 2012.
[30] N. E. Grant, F. E. Rougieux, D. Macdonald, J. Bullock, and Y. Wan, "Grown-in defects limiting the bulk lifetime of p-type float-zone silicon," *J. Appl. Phys.*, vol. 117, 2015, Art. no. 055711.
[31] R. A. Sinton and A. Cuevas, "Contactless determination of current-voltage characteristics and minority-carrier lifetimes in semiconductors from quasi-steady-state photoconductance data," *Appl. Phys. Lett.*, vol. 69, 1996, Art. no. 2510.
[32] L. J. Geerligs, G. Coletti, and D. Macdonald, "On accurate and quantitative measurements of iron-concentration in multicrystalline silicon by iron-boron pair dissociation," in *Proc. 21st Eur. Photovolt. Solar Energy Conf. Exhib.*, Dresden, Germany, Sep. 4–8, 2006, pp. 692–695.
[33] M. A. Jensen *et al.*, "Synchrotron-based analysis of chromium distributions in multicrystalline silicon for solar cells," *Appl. Phys. Lett.*, vol. 106, 2015, Art. no. 202104.
[34] J. Schmidt *et al.*, "Impurity-related limitations of next-generation industrial silicon solar cells," *IEEE J. Photovolt.*, vol. 3, no. 1, pp. 114–118, Jan. 2013.
[35] D. A. Iordache, P. E. Sterian, and I. Tunaru, "Charge coupled devices as particle detectors," *Adv. High Energy Phys.*, vol. 2013, 2013, Art. no. 425746.
[36] P. Deixler *et al.*, "Laplace-transform deep-level transient spectroscopy studies of the G4 gold-hydrogen complex in silicon," *Appl. Phys. Lett.*, vol. 73, no. 21, pp. 3126–3128, 1998.
[37] K. Graff, *Metal Impurities in Silicon-Device Fabrication*. New York, NY, USA: Springer, 2000.
[38] A. Cuevas, "The effect of emitter recombination on the effective lifetime of silicon wafers," *Sol. Energy Mater. Sol. Cells*, vol. 57, pp. 277–290, 1999.
[39] A. L. Blum *et al.*, "Interlaboratory study of eddy-current measurement of excess-carrier recombination lifetime," *IEEE J. Photovolt.*, vol. 4, no. 1, pp. 525–531, Jan. 2014.
[40] S. Boughaba and D. Mathiot, "Deep level transient spectroscopy characterization of tungsten-related deep levels in silicon," *J. Appl. Phys.*, vol. 69, pp. 278–283, 1991.
[41] G. Coletti, "Sensitivity of state-of-the-art and high efficiency crystalline silicon solar cells to metal impurities," *Prog. Photovolt.: Res. Appl.*, vol. 21, no. 5, pp. 1163–1170, 2013.
[42] A. E. Morishige *et al.*, "Synchrotron-based investigation of transition-metal getterability in n-type multicrystalline silicon," *Appl. Phys. Lett.*, vol. 108, 2016, Art. no. 202104.

Ashley E. Morishige received the Bachelor of Engineering degree from Thayer School of Engineering, Dartmouth, College, Hanover, NH, USA, in 2011 and the M.S. and Ph.D. degrees in mechanical engineering from the Massachusetts Institute of Technology, Cambridge, MA, USA, in 2013 and 2016, respectively.

Her current research interests include characterization, gettering, and simulation of trace metal impurities in crystalline silicon solar cells.

Mallory A. Jensen received the B.S. degree in mechanical engineering from the University of Pennsylvania, Philadelphia, PA, USA, in 2010 and the M.S. degree in mechanical engineering from the Massachusetts Institute of Technology, Cambridge, MA, USA, in 2015, where she is currently working toward the Ph.D. degree in mechanical engineering.

Her current research interests include lifetime spectroscopy for defect identification in crystalline silicon.

David Berney Needleman received the B.S. degree in physics from the University of Oregon, Eugene, OR, USA, in 2007 and the M.S. and Ph.D. degrees in mechanical engineering from the Massachusetts Institute of Technology, Cambridge, MA, USA, in 2014 and 2016, respectively.

He was a Research and Development Engineer with Atlantic Solar, Cape Town, South Africa. His current research interests include structural defects in crystalline silicon solar cells.

Kenta Nakayashiki received the B.S. degree from the University of Arizona, Tucson, AZ, USA, in 2002 and the Ph.D. degree from the Georgia Institute of Technology, Atlanta, GA, USA, in 2007, both in electrical engineering.

He is currently a Fellow in technology at REC Solar.

Jasmin Hofstetter received the B.Sc. degree in physics from Freie Universität Berlin, Berlin, Germany, in 2006 and the Ph.D. degree in photovoltaic solar energy from Universidad Politécnica de Madrid, Madrid, Spain, in 2011.

She joined the Photovoltaic Research Laboratory, Massachusetts Institute of Technology, Cambridge, MA, USA, as a Postdoctoral Research Scientist on a Feodor Lynen Postdoctoral Fellowship in 2011. She joined 1366 Technologies, Inc., Bedford, MA, as a Senior Process Engineer in 2014.

Tsu-Tsung Andrew Li received the B.E. degree in photovoltaics and solar energy from the University of New South Wales, Sydney, Australia, in 2006; the Ph.D. degree in engineering from the Australian National University, Canberra, Australia, in 2011; and the M.B.A. degree from the University of Oxford, Oxford, U.K., in 2015.

He was a Principal Engineer with the REC Solar Pte. Ltd., Singapore. He is currently the COO at Gyana Limited, London, U.K.: a data sciences startup that is building a machine-learning based platform to gather the enormous amount and the diversity of big data available and structure it into an intuitive representation of the world.

Tonio Buonassisi (M'13) received the Ph.D. degree in applied science and technology from the University of California at Berkeley, Berkeley, CA, USA, with additional research with the Fraunhofer Institute for Solar Energy Systems and the Max-Planck-Institute for Microstructure Physics.

He is currently the Head of the Photovoltaic Research Laboratory, Massachusetts Institute of Technology, Cambridge, MA, USA, which combines crystal growth, processing, characterization, defect simulation, and cost-performance modeling to engineer naturally abundant and manufacturable materials into cost-effective high-performance devices. His research interests include silicon (kerfless absorbers, advanced manufacturing, and defects), Earth-abundant thin films, and high-efficiency concepts.